IET Microwaves, Antennas & Propagation

Research Article

IET Journals
The Institution of Engineering and Technology

Rapid multi-objective design optimisation of compact microwave couplers by means of physics-based surrogates

ISSN 1751-8725
Received on 21st April 2015
Revised on 15th September 2015
Accepted on 28th October 2015
doi: 10.1049/iet-map.2015.0279
www.ietdl.org

Slawomir Koziel[1] ✉, *Adrian Bekasiewicz*[1], *Piotr Kurgan*[2], *John W. Bandler*[3]

[1]*Engineering Optimization and Modeling Center, School of Science and Engineering, Reykjavik University, Menntavegur 1 101 Reykjavik, Iceland*
[2]*Faculty of Electronics, Telecommunications and Informatics, Gdansk University of Technology, 80–233 Gdansk, Poland*
[3]*Department of Electrical and Computer Engineering, McMaster University, Hamilton, ON, Canada, L8S 4K1*
✉ *E-mail: koziel@ru.is*

Abstract: The authors introduce a methodology for fast multi-objective design optimisation of miniaturised microwave couplers. The approach exploits the surrogate-based optimisation paradigm with an underlying low-fidelity model constructed from an equivalent circuit of the structure under consideration, corrected through implicit and frequency space mapping. A fast prediction tool obtained this way is subsequently optimised by a multi-objective evolutionary algorithm to identify an initial approximation of the Pareto front, that is, a set of designs representing the best possible trade-offs between conflicting objectives. The correction/optimisation of the surrogate is then iterated by design space confinement and segmentation based on a Pareto set representation obtained thus far in the process. This aims at improving the surrogate model accuracy in the vicinity of the Pareto-optimal solutions. The technique is demonstrated by two design examples of compact rat-race couplers. Experimental validation is also provided.

1 Introduction

The design of compact microwave passive circuits for modern wireless communication systems requires handling of several, often conflicting objectives, including size, bandwidth (BW), and phase response [1–3]. For space-limited applications, finding an appropriate trade-off between structure size and its electrical performance is of particular interest. At the same time, as a result of highly compressed layouts (such as in fractal-shaped couplers [4], hybrids incorporating compact microstrip resonant cells [5], or circuits modified by defected ground structures [6]), a reliable evaluation of the miniaturised components cannot be realised by means of simplified representations, for example, equivalent circuits [7], because such models are incapable of adequately accounting for electromagnetic (EM) cross-couplings inside and between the elementary cells of the structure [3]. Accurate analysis can only be achieved by means of full-wave EM simulations. Unfortunately, high-fidelity EM simulations of compact circuits are CPU intensive. This high evaluation cost renders conventional design strategies (e.g. parameter sweeps [8], gradient-based search [9], global optimisation using population-based metaheuristics [10]) impractical.

These difficulties can be alleviated to some extent by the utilisation of adjoint sensitivities [11], which may lead to a considerable cost reduction when using gradient methods, as demonstrated in the case of microwave filters [12] or antennas [13]. Another approach that has gained considerable attention in recent years is surrogate-based optimisation (SBO) [14–18]. In SBO, the key idea behind reducing the cost of the simulation-driven design process is that of replacing the direct optimisation of the expensive high-fidelity EM model by the iterative enhancement and re-optimisation of its computationally cheap representation (a surrogate). Probably the most popular method of this kind in microwave engineering is space mapping (SM) [14, 19, 20]. Many SM applications take advantage of available equivalent circuit models, for example, in the design of filters [21], multiplexers [22], or impedance transformers [15]. Other popular SBO methods include adaptive response correction [23], manifold mapping [24], shape-preserving response correction [25], adaptively adjusted design specifications [26], and multi-fidelity algorithms [27]. Some of these methods and their modifications have been developed to address issues related to expensive low-fidelity models (e.g. simplified representations of antenna structures are normally constructed from coarse-discretisation EM simulations [28, 29]).

Compact microwave components are typically developed exploiting novel topologies so that the relationship between the structure size and its electrical performance is difficult to predict. Sufficient insight into these relationships as well as possible trade-offs between various design objectives can be obtained through multi-objective optimisation [28]. The outcome of a multi-objective optimisation process is a set of alternative designs representing the best possible trade-offs between conflicting objectives (referred to as a Pareto set), which – for compact microwave structures – would often be the circuit size and one or more electrical performance parameters [29, 30]. The most popular solution approaches to generating Pareto-optimal designs are population-based metaheuristics [10], including evolutionary algorithms [31], and particle swarm optimisers [32]. Clearly, direct simulation-driven metaheuristic optimisation of compact circuits is not possible due to the excessive computational cost related to the number of objective function evaluations required in the process (typically, thousands, tens of thousands, or more).

In this paper, we propose an efficient procedure for multi-objective EM-driven design of compact microwave couplers. Our approach utilises fast equivalent circuit models enhanced by frequency scaling and implicit SM [14, 20, 33, 34], a multi-objective evolutionary algorithm (MOEA), as well as iterative surrogate model refinement involving design space confinement and segmentation (based on the currently known Pareto set representation). These measures allow us to overcome the problem of the poor quality of an equivalent circuit model: although the generalisation capability of the initial (space-mapping-corrected) surrogate is relatively poor, it is gradually improved by focusing model correction (mapping update) in the region containing the Pareto-optimal solution, with the simultaneous restriction of the search space to that region. An important component of our design process is the appropriate handling of multiple objectives, which is partially built into the selection procedure of the evolutionary algorithm. Our technique is verified by

two design examples of compact microwave couplers, that is, a rat-race coupler (RRC) with folded transmission lines (TLs), and a RRC with shunt-stub-based TLs. The proposed method is also validated by physical measurements of the fabricated RRC prototypes extracted from the Pareto set pertaining to one of the available examples.

2 Design optimisation methodology

In this section, we formulate the multi-objective optimisation problem, and describe the main components of the proposed design procedure. We also explain our way of handling the design objectives, as well as the space-mapping correction of the low-fidelity model. A discussion of the overall flow of the optimisation process is also provided.

2.1 Multi-objective optimisation problem formulation

Let $F_k(\boldsymbol{R}_f(\boldsymbol{x}))$, $k = 1,\ldots, N_{obj}$, denote the design criteria for the problem at hand. Multi-objective optimisation aims at identifying a representation of a so-called Pareto-optimal set X_P that contains non-dominated designs such that for any $\boldsymbol{x} \in X_P$, there is no other design $\boldsymbol{y}$ for which the relation $\boldsymbol{y} < \boldsymbol{x}$ is satisfied ($\boldsymbol{y} < \boldsymbol{x}$, i.e. $\boldsymbol{y}$ dominates over $\boldsymbol{x}$, if $F_k(\boldsymbol{R}_f(\boldsymbol{y})) \leq F_k(\boldsymbol{R}_f(\boldsymbol{x}))$ for all $k = 1,\ldots, N_{obj}$, and $F_k(\boldsymbol{R}_f(\boldsymbol{y})) < F_k(\boldsymbol{R}_f(\boldsymbol{x}))$ for at least one k) [10, 35]. The elements of X_P represent the best possible trade-offs between the (usually conflicting) objectives F_k.

2.2 Design objectives for compact microwave couplers

The design of microwave couplers typically involves multiple objectives that are hard to obtain for miniaturised structures. Traditionally, these include: matching of the input port, obtaining half-power at the output ports with a certain phase shift, and isolating the remaining port. In the case of conventional couplers, the above objectives are satisfied exclusively at the centre frequency. For compact structures, however, it is crucial to consider a wider range of frequencies as the BW of a compact coupler tends to be narrowed-down with smaller and smaller size of the circuit. Thus, our main goal is to find the best possible trade-offs between the size of the compact coupler and its BW, while ensuring its proper operation in the vicinity of the centre frequency. Therefore, we formulate two primary design objectives:

- F_1 – BW maximisation (the BW is defined as the range of frequencies for which both $|S_{11}|$ and $|S_{41}|$ are below –20 dB),
- F_2 – size minimisation (layout area).

At the same time, we consider two auxiliary objectives to ensure a proper operation of the coupler at hand:

- F_3 – the power split error between the output ports at the operating frequency (defined as $| |S_{21}| - |S_{31}| |$),
- F_4 – the BW symmetry (defined as the ratio between the wider and narrower parts of the previously-defined BW with respect to the operating frequency).

The primary objectives are handled explicitly by the multi-objective optimisation algorithm (cf. Section 2.3). The other two objectives are treated as constraints, and are incorporated into the selection mechanism of the evolutionary algorithm.

2.3 Multi-objective evolutionary algorithm primary and auxiliary objectives

The main optimisation engine utilised in this work is a MOEA. To make the optimisation process computationally feasible, MOEA cannot directly handle the CPU-intensive high-fidelity EM model of the structure (denoted as $\boldsymbol{R}_f$) as the typical number of objective function evaluations in such as a process is in thousands, tens or even hundreds of thousands. Instead, the algorithm optimises the surrogate model of the structure (termed $\boldsymbol{R}_s$), which is a fast representation of $\boldsymbol{R}_f$ (typically, an equivalent circuit model). The surrogate is iteratively refined so that it gradually becomes a better approximation of the high-fidelity model, at least in the vicinity of the Pareto front.

Here, we use a rather standard MOEA implementation, with fitness sharing, mating restrictions and Pareto-dominance tournament selection [10], as the mechanisms pushing the solutions towards the Pareto front. Formally, MOEA works with all four objectives (both primary and auxiliary, as described in Section 2.2), however, we are only interested in that part of the Pareto front for which the latter objectives satisfy certain thresholds (cf. Section 3.1). These conditions are enforced at the selection stage of the evolutionary algorithm, where the fitness $f(\boldsymbol{x})$ value assigned to a solution $\boldsymbol{x}$ (based on its Pareto ranking and fitness sharing) is reduced using the following penalty term

$$f(\boldsymbol{x}) \leftarrow f(\boldsymbol{x}) - \sum_{k=1}^{2} \beta_k \max\left(\frac{(F_{k+2}(\boldsymbol{R}_f(\boldsymbol{x})) - F_{k+2.\max})}{F_{k+2.\max}, 0}\right)^2 \quad (1)$$

where $F_{3.max}$ and $F_{4.max}$ are the threshold values for the power split error and BW symmetry, respectively; penalty factors β_k are set experimentally. Due to (1), the solutions that violate given thresholds for the auxiliary objectives tend to be eliminated from the population processed by MOEA, so that towards the end of the optimisation task, the majority of the population satisfies these conditions.

This approach is significantly more efficient than the explicit handling of all four objectives. In the latter case, the Pareto front would be a three-dimensional manifold in the feature space. The acceptable part of it (i.e. the one containing solutions that satisfy the aforementioned conditions regarding the power split and the BW symmetry) would be a one-dimensional subset that could not be appropriately represented in the Pareto set produced by MOEA (even for relatively large population size of, say, a few hundred individuals).

2.4 Low-fidelity model correction design space confinement

In this work, the surrogate model $\boldsymbol{R}_s$ of the structure at hand is constructed by correcting its low-fidelity model (denoted $\boldsymbol{R}_c$) using frequency and implicit space mapping [14, 20, 33, 34]. This particular choice of possible SM transformations is the result of initial experiments as well as the fact that a frequency shift is one of the major types of misalignment between the equivalent circuit model $\boldsymbol{R}_c$ and the high-fidelity model $\boldsymbol{R}_f$. The surrogate is defined as

$$\boldsymbol{R}_s(\boldsymbol{x}) = \boldsymbol{R}_{c.F}(\boldsymbol{x}; \boldsymbol{f}, \boldsymbol{p}) \quad (2)$$

where $\boldsymbol{R}_{c.F}$ is a frequency-scaled low-fidelity model (an equivalent circuit), while $\boldsymbol{f}$ and $\boldsymbol{p}$ are frequency space mapping and implicit space mapping parameters, respectively.

The frequency and implicit SM are implemented as follows. Let $\boldsymbol{R}_c(\boldsymbol{x}) = [R_c(\boldsymbol{x}, \omega_1)\ R_c(\boldsymbol{x}, \omega_2) \ldots R_c(\boldsymbol{x}, \omega_m)]^T$, where $R_c(\boldsymbol{x}, \omega_j)$ is an evaluation of the circuit model at a frequency ω_j. Then, $\boldsymbol{R}_{c.F}(\boldsymbol{x}; \boldsymbol{f}, \boldsymbol{p}) = [R_c(\boldsymbol{x}, f_0 + \omega_1 \cdot f_1, \boldsymbol{p}) \ldots R_c(\boldsymbol{x}, f_0 + \omega_m \cdot f_1, \boldsymbol{p})]^T$, with f_0 and f_1 being the frequency scaling parameters. Here, the implicit SM parameters $\boldsymbol{p}$ are dielectric permittivity and substrate thickness of the microstrip components of the circuit corresponding to $\boldsymbol{p} = [\varepsilon_1\ \varepsilon_2\ \varepsilon_3 \ldots h_1\ h_2\ h_3 \ldots]^T$ (see, e.g. Fig. 1*a*). The assignment of these parameters to specific parts of the equivalent circuit is guided by engineering experience. The SM parameters are extracted to minimise misalignment between $\boldsymbol{R}_s$ and $\boldsymbol{R}_f$ in the norm sense:

$$[\boldsymbol{f}^*, \boldsymbol{p}^*] = \arg\min_{\boldsymbol{f}, \boldsymbol{p}} \sum_{\boldsymbol{x} \in X_B} ||\boldsymbol{R}_f(\boldsymbol{x}) - \boldsymbol{R}_{c.F}(\boldsymbol{x}; \boldsymbol{f}, \boldsymbol{p})|| \quad (3)$$

Here, X_B denotes a set of training points. There are two types of training sets utilised to construct the surrogate. The parameter extraction carried out to obtain the initial surrogate model $\boldsymbol{R}_s^{(0)}$ is

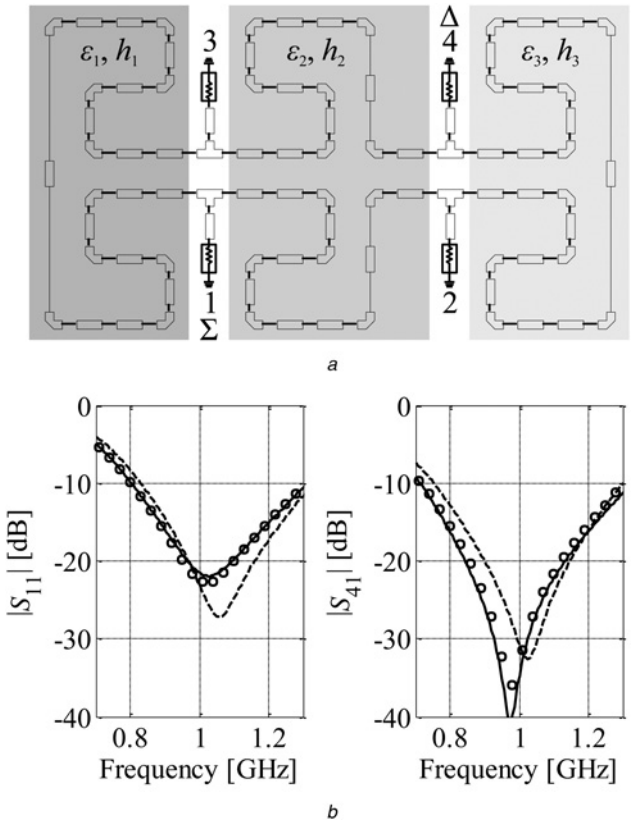

Fig. 1 *Compact RRC*

a Equivalent circuit (low-fidelity model) of the compact RRC of Section 3.1. Highlighted regions correspond to different sets of implicit SM parameters p, i.e., permittivity and thickness of the substrate (cf. Section 2.4)
b Return loss and isolation against frequency for variable-fidelity models of a compact RRC of Section 3.1 (low-fidelity (– –), surrogate (o), and high-fidelity (—) models) at a certain design $\boldsymbol{x}$ (other than at which the surrogate was extracted)

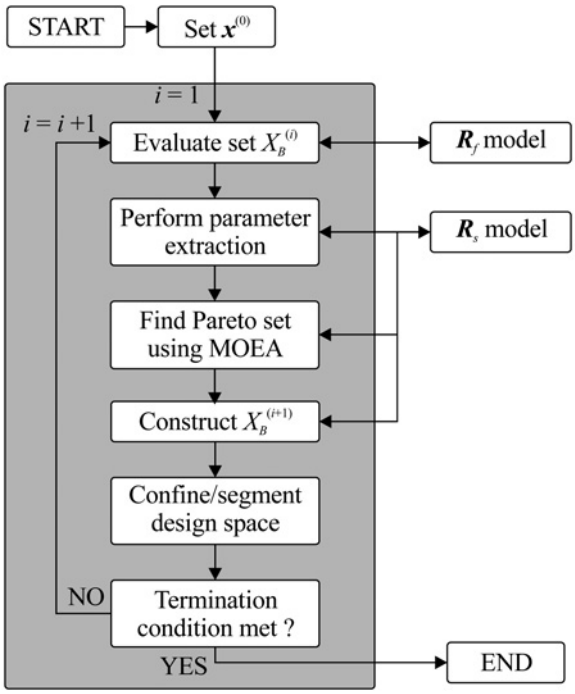

Fig. 2 *Flowchart of the multi-objective design procedure*

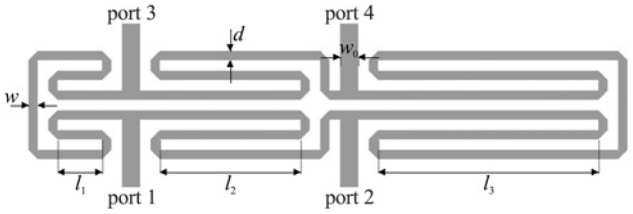

Fig. 3 *Design case 1: Layout of the compact RRC composed of folded TLs*

executed using the star-distribution base set [36, 37] allocated in the original design space. Typically, surrogate model accuracy is limited because lower/upper bounds are normally set up to be wider rather than narrower in order to make sure that the entire Pareto front can be captured within the prescribed bounds. After MOEA optimisation of $\boldsymbol{R}_s^{(0)}$, the design space is confined by narrowing the bounds so that the reduced space only contains the Pareto set and its small vicinity. Due to this, the next surrogate model – with the parameter extraction process based on the $\boldsymbol{R}_f$ points sampled along the Pareto set found so far – is expected to be more accurate. If necessary, a segmentation process can also be utilised, where the design space is divided into two or more compartments with respect to the dimension showing the largest variations in the structure's response. Subsequently, the parameter extraction process is executed separately in each compartment. The entire process is automated through appropriate implementation.

Fig. 1*b* shows exemplary responses (here, only $|S_{11}|$ and $|S_{41}|$ are shown for clarity) of the high- and low-fidelity models at a selected design $\boldsymbol{x}$, as well as the response of the surrogate model $\boldsymbol{R}_s^{(1)}$ at the same design. It can be observed that despite of relatively large discrepancies between the low- and high-fidelity models, both the approximation and generalisation capability of the surrogate is

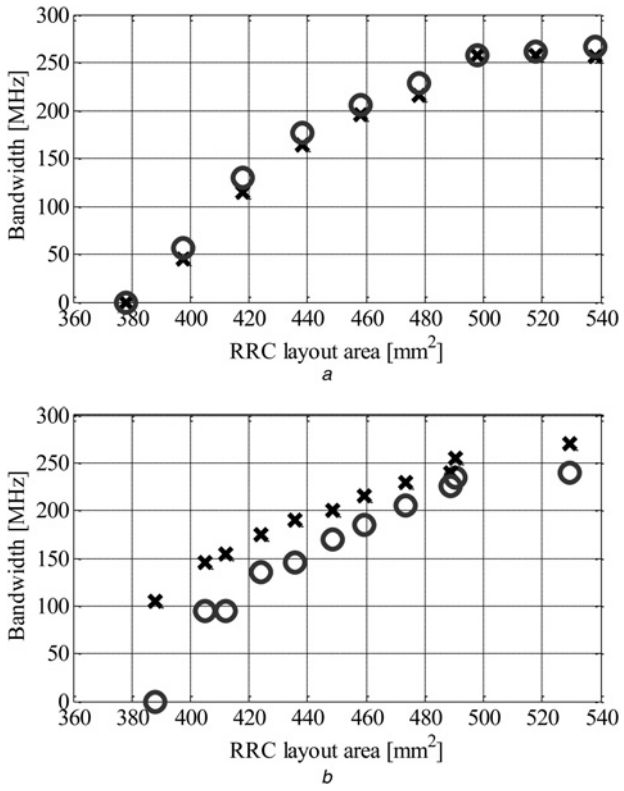

Fig. 4 *Design case 1: Pareto set representations found by means of*

a Complete multi-objective optimisation procedure of Section 2
b Its limited version without design space confinement for surrogate model parameter extraction. Markers denote the surrogate model (×), and high-fidelity model (○) responses. The latter are included for verification purposes

Table 1 Design case 1: selected optimisation results

Design variables, mm					Objectives		Miniaturisation[a], %
l_1	l_2	l_3	d	W	BW, MHz	RRC layout area, mm^2	
4.82	14.67	22.20	0.800	0.867	267	538	88.2
4.43	14.71	21.76	0.784	0.849	262	518	88.6
4.34	14.41	21.32	0.768	0.832	258	498	89.0
4.42	13.39	22.03	0.746	0.808	228	477	89.5
4.35	13.19	21.99	0.724	0.784	206	458	89.9
4.36	12.73	22.01	0.702	0.761	176	438	90.3
4.29	12.15	22.09	0.681	0.738	130	417	90.8
4.16	11.79	21.89	0.661	0.716	56	397	91.2
4.05	11.19	21.87	0.641	0.695	0	378	91.7

[a]With respect to conventional RRC (size: 47.5 × 95.5 = 4536 mm^2)

good. Note that $\boldsymbol{R}_s^{(1)}$ is created in the vicinity of the initial Pareto front approximation found by the evolutionary algorithm.

2.5 Optimisation algorithm

The overall flow of the multi-objective optimisation procedure is as follows (the initial training set $X_B^{(0)}$ is a star-distribution set [36, 37]):

i. Set iteration index $i = 0$.
ii. Evaluate $\boldsymbol{R}_f$ at the training set $X_B^{(i)}$.
iii. Perform parameter extraction (3) to find the surrogate $\boldsymbol{R}_s^{(i)}$.
iv. Optimise $\boldsymbol{R}_s^{(i)}$ using MOEA to find a Pareto set.
v. Sample the Pareto set to get a new training set $X_B^{(i+1)}$.
vi. Confine/segment the design space.
vii. If $\max\{\boldsymbol{x} \in X_B^{(i)} : \|\boldsymbol{R}_f(\boldsymbol{x}) - \boldsymbol{R}_s^{(i)}(\boldsymbol{x})\|\} < \varepsilon$ then| END; else set $i = i + 1$ and go to 2.

The termination condition measures the accuracy of the current surrogate model along the Pareto front representation obtained in a given iteration. Good accuracy indicates convergence to a true front, which terminates the optimisation process. The flowchart of the multi-objective design optimisation process is shown in Fig. 2.

It should be mentioned that it is also possible to exploit adjoint sensitivities (if available) to refine the Pareto front starting from its initial approximation obtained in the first execution of Step 4 of the algorithm. To this end, the front would have to be sampled and the respective designs would have to be tuned through constrained gradient search (e.g. by improving one of the objectives without degrading the remaining ones). On the other hand, such a procedure would only produce a discrete representation of the Pareto front at a cost comparable with that of the proposed algorithm. The benefit would be better precision in identifying the Pareto-optimal designs.

3 Case studies

In this section, we use the design methodology of Section 2 to perform a fast multi-objective optimisation of compact microwave couplers. To demonstrate the application of the proposed approach, we consider two design examples, namely, a RRC with folded TLs, and an RRC with shunt-stub-based TLs. For each case study, a set of nine alternative design solutions is shown, illustrating the best possible trade-offs between conflicting objective of size and BW. Note that the miniaturisation level of each design solution is calculated with respect to a conventional equal-split RRC of rectangular shape [5] that occupies 4536 mm^2 with external dimensions of 47.5 mm × 95.5 mm.

3.1 Design case 1: compact RRC with folded TLs

The first design example is an RRC, whose footprint is simply miniaturised by folding each of its quarter-wave TLs to the interior (see Fig. 3). We choose Taconic RF-35 dielectric substrate (ε_r = 3.5, h = 0.762 mm, tanδ = 0.018) for circuit implementation. The

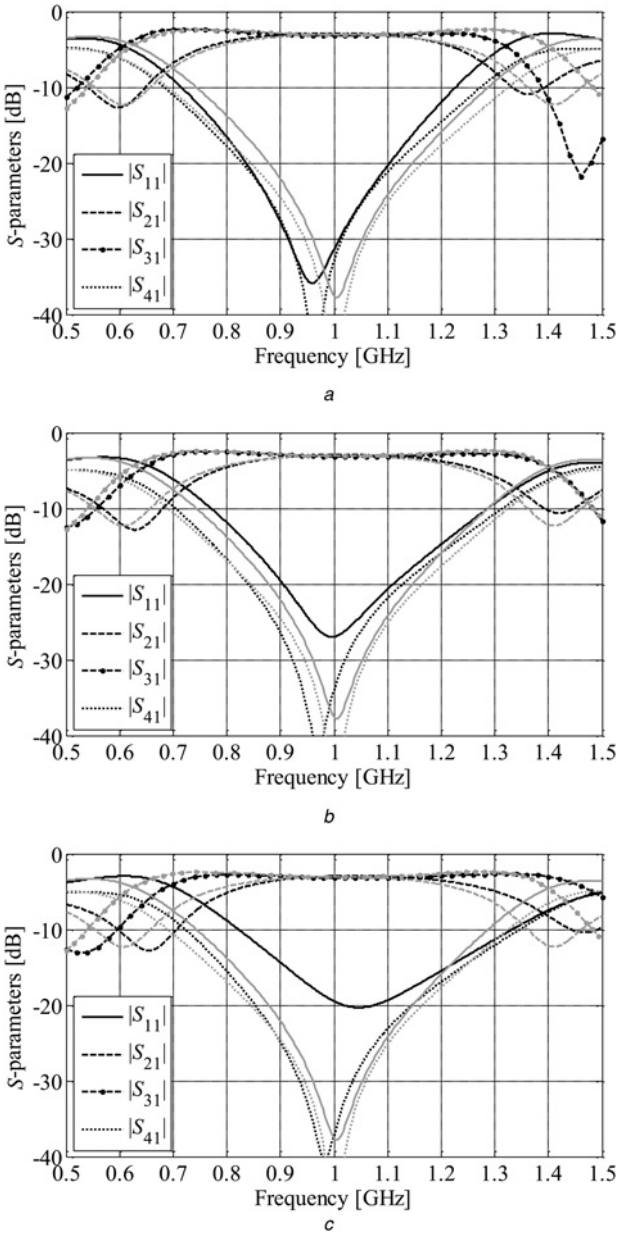

Fig. 5 *Design case 1: S-parameters vs. frequency for the selected designs corresponding to the layout areas of*

a 538 mm^2
b 458 mm^2
c 397 mm^2. Black and grey curves represent the performance of a given compact coupler, and a conventional one, respectively. The latter has been designed for comparison purposes

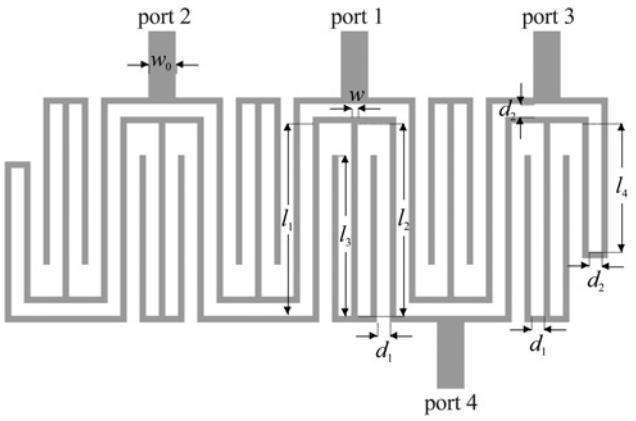

Fig. 6 *Design case 2: Layout of the compact RRC with shunt-stub-based TLs [1]*

compact coupler of Fig. 1*a* is intended to operate in the vicinity of 1 GHz frequency. The structure is characterised by five independent design parameters: $\boldsymbol{x} = [l_1\ l_2\ l_3\ d\ w]^T$, with w_0 fixed to 1.7 mm to ensure a 50-ohm input impedance. The footprint of this coupler is taken as an $A \times B$ rectangle, where $A = 6w + 5d$ and $B = 8w + 7d + l_1 + l_2 + l_3$. Lower/upper bounds $\boldsymbol{l}/\boldsymbol{u}$ of the solution space are given by: $\boldsymbol{l} = [2\ 10\ 17\ 0.2\ 0.5]^T$ and $\boldsymbol{u} = [8\ 16\ 25\ 1.2\ 1.5]^T$. All the above dimensions are in millimetres.

The high-fidelity EM model $\boldsymbol{R}_f$ of the coupler is implemented in CST Microwave Studio [38], and contains approximately 220,000 mesh cells, which translates into about 15 min of simulation time per design. The low-fidelity model $\boldsymbol{R}_c$ of the coupler under discussion is an equivalent circuit implemented in Agilent ADS [39]. The schematic diagram of this circuit is shown in Fig. 1*a*. It should be noted that the substrate of the low-fidelity model has been divided into three sections, for which a set of implicit parameters (the substrate height h_k, and permittivity ε_k, $k = 1, 2, 3$) can be defined independently as explained in Section 2.4.

The values of the auxiliary objectives defined in Section 2.2 are to be kept below $F_{3,\max} = 0.2$ dB, and $F_{4,\max} = 1.5$ for power split error and BW symmetry, respectively. Note that $F_3 = 0$ dB corresponds to a perfect (equal-split) power division between the output ports, whereas $F_4 = 1$ represents perfect symmetry around the centre frequency (here, 1 GHz). Penalty factors of (1) are set to 10.

The RRC of Fig. 3 has been optimised in a multi-objective sense using the technique introduced in Section 2. The final Pareto set has been obtained in three iterations of the proposed procedure. An inspection of Fig. 4*a* reveals that the differences between the surrogate and high-fidelity model samples allocated along the front are minor (below 15 MHz BW-wise). For comparison purposes, the same example has been optimised without the iterative confinement of the design space (cf. Section 2.4, stage 6). The surrogate model used in this process is built using star-distribution training points allocated in the original design space. As a result, the final Pareto set of Fig. 4*b*, corresponding to the surrogate model, illustrates much larger discrepancies in comparison with its

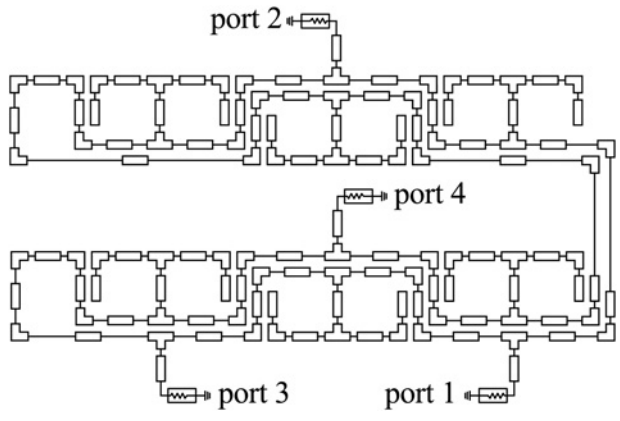

Fig. 7 *Design case 2: Equivalent circuit (low-fidelity model) of the compact RRC of Fig. 6*

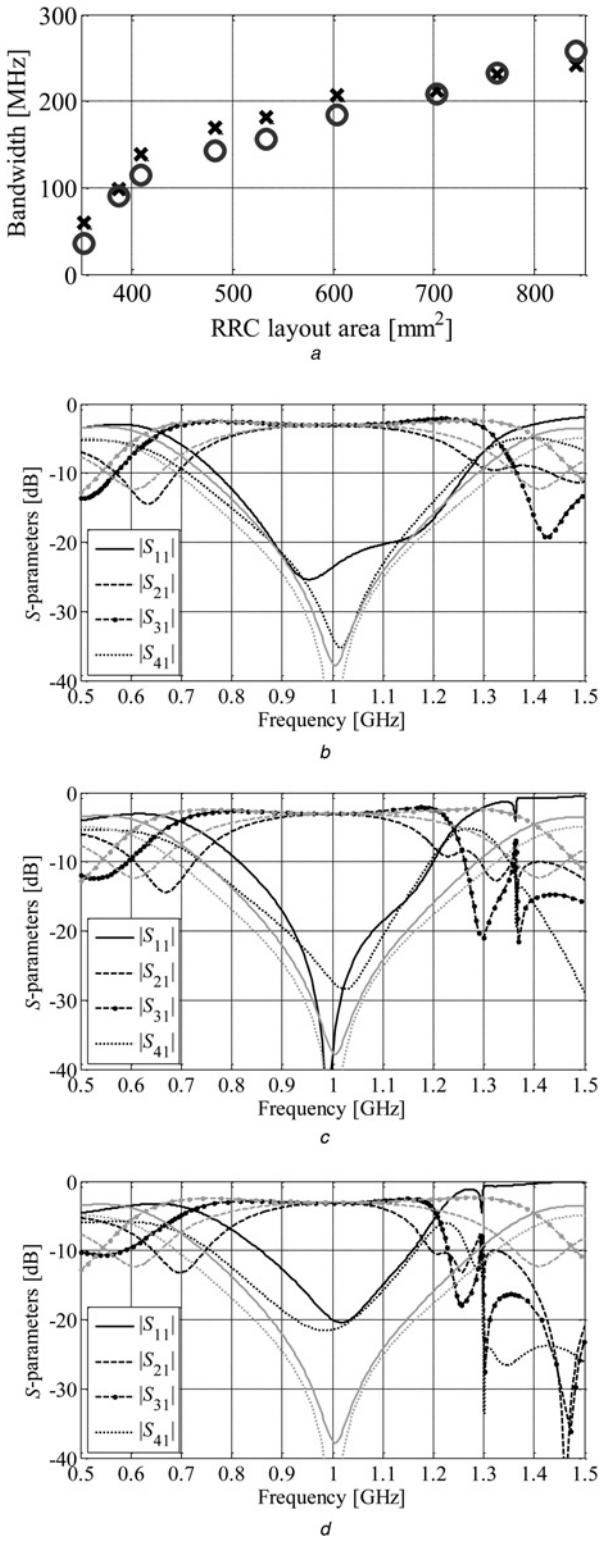

Fig. 8 *Design case 2*

a Pareto set representation with the accuracy of the surrogate (×) and high-fidelity (○) model; *S*-parameters vs. frequency for the selected designs of the compact RRCs of: a 841 mm^2
b 534 mm^2
c 353 mm^2 areas (black lines). Grey lines represent the response of a conventional coupler

Table 2 Design case 2: selected optimisation results

Design variables, mm							Objectives		Miniaturisation[a], %
w	d_1	d_2	l_1	l_2	l_3	l_4	BW, MHz	RRC layout area, mm^2	
0.61	0.3	2.90	13.16	13.16	1.55	0.83	258	841	81.5
0.55	0.3	2.60	13.50	13.50	3.85	1.71	232	763	83.2
0.50	0.27	2.07	15.44	15.44	6.11	3.03	208	703	84.5
0.45	0.2	2.07	14.52	14.52	9.09	2.87	184	604	86.7
0.39	0.2	1.93	14.23	14.23	12.57	3.09	156	534	88.2
0.37	0.17	1.71	14.51	14.51	14.36	8.11	143	483	89.4
0.35	0.15	1.26	15.00	15.00	14.85	6.21	114	409	91.0
0.31	0.15	1.20	15.53	15.53	15.37	5.78	90	387	91.5
0.28	0.15	1.07	15.71	15.71	15.55	6.02	36	353	92.2

[a]With respect to conventional RRC (size: 47.5 × 95.5 = 4536 mm^2)

high-fidelity counterpart than previously (the worst case shows more than 100 MHz BW dissimilarity). These results indicate that the iterative confinement of the solution space for enhanced parameter extraction significantly increases the accuracy of the space-mapping-corrected surrogate. Selected optimisation results, including final designable parameters, and their corresponding figures of merit (BW, size, and miniaturisation), are listed in Table 1. Fig. 5 shows the S-parameter plots for three selected designs (two extreme points and the middle point from Table 1), compared with the transmission characteristics of a conventional RRC. One can observe that both the miniaturisation and design method contribute to discrepancies in the performance between the conventional coupler and its compact versions. More specifically, the former clearly leads to the BW degradation (especially for more and more compact designs, as in Figs. 5*b* and *c*), while the latter results in a shift of the $|S_{11}|$ and $|S_{41}|$ minimums (the exact location of the $|S_{11}|$ and $|S_{41}|$ minimums is not controlled by the proposed method).

The obtained results show that the design objectives are indeed conflicting. In particular, the overall footprint of the structure with the broadest BW of 267 MHz simultaneously exhibits the largest footprint of 538 mm^2. The smallest coupler design that fulfils the BW criterion is 397 mm^2 (which translates into a 56-MHz BW). It should be emphasised that the RRC BW and footprint vary by 79 and 26% along the Pareto front, respectively. Moreover, it is noteworthy that all optimal designs satisfy the prescribed constraints concerning the power split error and BW symmetry.

The computational cost of the entire design process is very low, especially considering the complexity of the multi-objective optimisation problem. Construction of the initial surrogate model requires 11 $\boldsymbol{R}_f$ samples (star distribution), whereas each algorithm iteration requires about 10 $\boldsymbol{R}_f$ samples. Thus, the total number of high-fidelity model evaluations is around 40. The overhead related to the parameter extraction process and surrogate model optimisation using MOEA is less than 50% of the overall cost. The aggregated cost of the proposed design procedure corresponds to less than 80 evaluations of $\boldsymbol{R}_f$ (about 20 h of CPU time). The multi-objective optimisation method introduced in this work has been compared with conventional MOEA optimisation based on direct evaluations of high-fidelity coupler model. Assuming a population of 500 individuals and 50 generations of MOEA, the estimated cost of direct multi-objective optimisation of the high-fidelity model $\boldsymbol{R}_f$ is over 260 days of the CPU time. This estimation is based on the number of objective function evaluations required by MOEA optimisation of the response surface approximation model. The overall CPU time required by our methodology is considerably lower, which means that comprehensive information on the miniaturised coupler may be obtained without involving excessive computational resources.

3.2 Design case 2: compact RRC with shunt-stub-based TLs

The second design example, shown in Fig. 6, is an RRC built from folded TLs loaded by shunt, T-shaped stubs. We use here the same dielectric substrate and design specifications as in the previous example. The structure is described by seven design parameters: $\boldsymbol{x} = [w\ d_1\ d_2\ l_1\ l_2\ l_3\ l_4]^T$. The width of the feeding line has been fixed to $w_0 = 1.7$ mm to ensure a 50-ohm input impedance. The

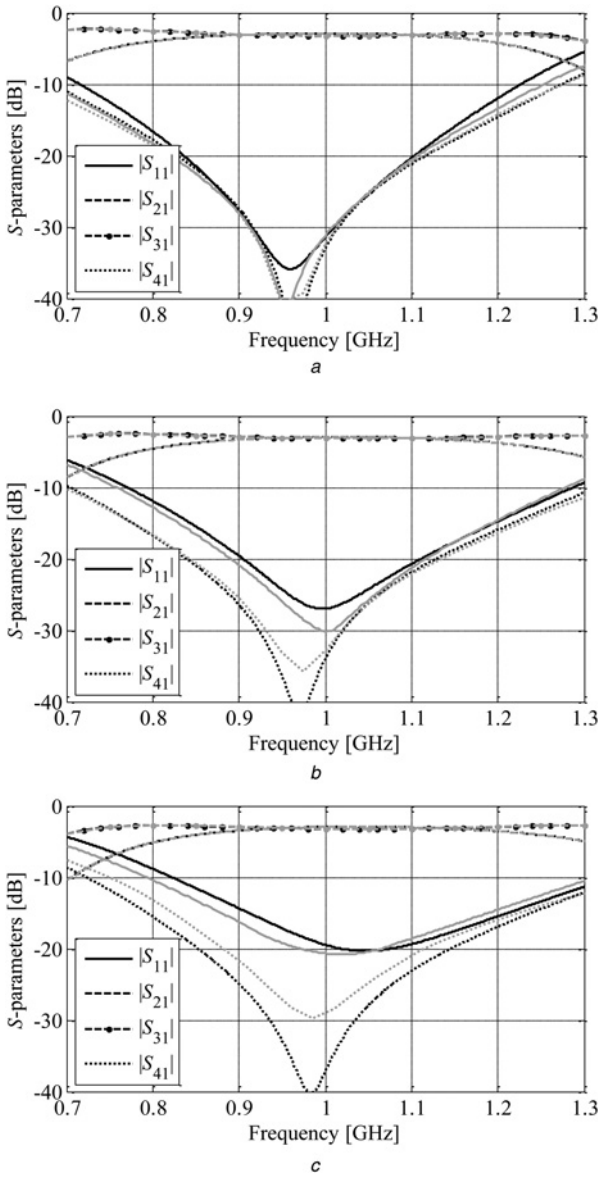

Fig. 9 *Comparison of the simulated (black curves) and measured (grey curves) frequency characteristics of the selected coupler designs with areas of*
a 538 mm^2
b 458 mm^2
c 397 mm^2

area of this coupler is given by $A \times B$, where $A = 32w + 24d_1 + 7d_2$ and $B = 3w + d_2 + l_1$. Lower/upper bounds $\boldsymbol{l}/\boldsymbol{u}$ of the solution space pertaining to this example are: $\boldsymbol{l} = [0.2\ 0.1\ 0.1\ 10\ 10\ 0.1\ 0.1]^T$ and $\boldsymbol{u} = [1.5\ 1.2\ 4\ 20\ 20\ 20\ 20]^T$. All the above dimensions are in millimetres.

The low-fidelity model $\boldsymbol{R}_c$ representing the coupler of Fig. 6 is an equivalent circuit implemented in Agilent ADS [39]. Its schematic diagram is illustrated in Fig. 7. The high-fidelity EM model $\boldsymbol{R}_f$ of the given coupler is implemented in CST Microwave Studio [38], and contains about 350,000 mesh cells, which translates into 25 min of simulation time per design. The auxiliary objectives used here have the same threshold level values as in the previous example.

We have executed the proposed method to perform a multi-objective optimisation of the coupler at hand, obtaining the final Pareto set in three iterations. The results shown in Fig. 8*a* indicate that the differences between the responses of the surrogate and high-fidelity models are rather small (maximal discrepancy is below 25 MHz BW-wise). Please note that the average misalignments are slightly elevated when compared with the previous example. This can be explained by the much more complex geometry of the given coupler, which results in less accurate low-fidelity model. Table 2 contains detailed data on the alternative design solutions, which illustrate the non-commensurable nature of the investigated dependence of size and BW. Transmission characteristics of the selected designs are shown in Figs. 8*b–d*. The performance of the conventional coupler has been added as a reference. As previously, the largest coupler with a footprint of 841 mm^2 exhibits the broadest BW of 258 MHz, while the smallest one (353 mm^2 area) features a BW of only 36 MHz. The narrowing-down of the BW is a direct result of miniaturisation, whereas shifting of the $|S_{11}|$ and $|S_{41}|$ minimums can be attributed to the design method itself. Please note that each design solution satisfies the performance constraints as defined beforehand. The variation of the respective design objectives along the Pareto front is 59% for the area, and 86% for the BW.

The overall cost of the design process is about 90 $\boldsymbol{R}_f$ simulations, which corresponds to around 38 hours of CPU time. A detailed cost breakdown is the following: 15 $\boldsymbol{R}_f$ evaluations for the construction of the initial surrogate model, and a total of 30 $\boldsymbol{R}_f$ simulations for its further refinement during the optimisation process (three algorithm iterations), as well as about 50 percent overhead with respect to $\boldsymbol{R}_f$ simulations for parameter extraction and MOEA optimisation of the surrogate.

4 Experimental verification

The selected Pareto-optimal designs of the coupler of Section 3.1, namely, (i) 538 mm^2, (ii) 458 mm^2, and (iii) 397 mm^2, have been fabricated (see Table 1 for detailed dimensions as well as corresponding objective function values). It should be noted that, in contrast with, for example, miniaturised couplers based on compact microstrip resonant cells [5, 40], our folded design is rather insensitive to fabrication inaccuracies. The manufactured RRCs have been measured and compared against EM simulations (see Fig. 9). The difference between the BWs of the selected couplers is 17, 19, and 38 MHz for the first, second, and third design, respectively. Overall, the measurement results are in good agreement with theoretical predictions. Slight discrepancies arise from the simplified EM model of the structures that lacks connectors, and uses isotropic dielectric substrates.

5 Conclusion

In this work, a procedure for fast multi-objective design optimisation of miniaturised microwave circuits is proposed. The main elements of our methodology, critical for its computational efficiency, include a combination of equivalent circuit modelling, SM, evolutionary algorithms, as well as iterative design space confinement and segmentation. Constraining the region of the design space in which the surrogate model is updated only to the vicinity of the current Pareto front representation allows us to maintain good approximation and generalisation capabilities of the model. Consequently, the algorithm is able to generate a reliable representation of the Pareto-optimal designs representing the best possible trade-offs between the conflicting objectives for the structure under consideration. The procedure has been demonstrated using two numerical examples of compact RRCs. The selected designs have been fabricated and measured, confirming the correctness of the proposed approach.

6 Acknowledgments

The authors thank Computer Simulation Technology AG, Darmstadt, Germany, for making CST Microwave Studio available. This work was supported in part by the Icelandic Centre for Research (RANNIS) Grant 130450051, by the National Science Center, Poland, under Grants 2013/11/B/ST7/04325 and 2014/12/T/ST7/00045, by the Natural Sciences and Engineering Research Council of Canada under Grants RGPIN7239–11 and STPGP447367-13, and by Bandler Corporation.

7 References

1 Tseng, C.-H., Chen, H.-J.: 'Compact rat-race coupler using shunt-stub-based artificial transmission lines', *IEEE Microw. Wirel. Compon. Lett.*, 2008, **18**, (11), pp. 734–736
2 Kim, T.-G., Lee, B.: 'Metamaterial-based wideband rat-race hybrid coupler using slow wave lines', *IET Microw., Antennas Propag.*, 2010, **4**, (6), pp. 717–721
3 Koziel, S., Kurgan, P., Pankiewicz, B.: 'Cost-efficient design methodology for compact rat-race couplers', *Int. J. RF Microw. Comput.-Aided Eng.*, 2014, **25**, pp. 236–242
4 Kurgan, P., Kitlinski, M.: 'Slow-wave fractal-shaped compact microstrip resonant cell', *Microw. Opt. Techn. Lett.*, 2010, **52**, (11), pp. 2613–2615
5 Bekasiewicz, A., Kurgan, P.: 'A compact microstrip rat-race coupler constituted by nonuniform transmission lines', *Microw. Opt. Tech. Lett.*, 2014, **56**, (4), pp. 970–974
6 Kurgan, P., Filipcewicz, J., Kitlinski, M.: 'Design considerations for compact microstrip resonant cells dedicated to efficient branch-line miniaturization', *Microw. Opt. Tech. Lett.*, 2012, **54**, (8), pp. 1949–1954
7 Liao, S.-S., Sun, P.-T., Chin, N.-C., *et al.*: 'A novel compact-size branch-line coupler', *IEEE Microw. Wirel. Compon. Lett.*, 2005, **15**, (9), pp. 588–590
8 Opozda, S., Kurgan, P., Kitlinski, M.: 'A compact seven-section rat-race hybrid coupler incorporating PBG cells', *Microw. Opt. Techn. Lett.*, 2009, **51**, (12), pp. 2910–2913
9 Nocedal, J., Wright, S.J.: 'Numerical optimization' (Springer Series in Operations Research, Springer, 2000)
10 Deb, K.: 'Multi-objective optimization using evolutionary algorithms' (John Wiley & Sons, New York, 2001)
11 Cheng, Q.S., Bandler, J.W., Koziel, S., *et al.*: 'The state of the art of microwave CAD: EM-based optimization and modeling', *Int. J. RF Microw. Comput.-Aided Eng.*, 2010, **20**, (5), pp. 475–491
12 Koziel, S., Ogurtsov, S., Bandler, J.W., *et al.*: 'Reliable space-mapping optimization integrated with EM-based adjoint sensitivities', *IEEE Trans. Microw. Theory Tech.*, 2013, **61**, (10), pp. 3493–3502
13 Sabbagh, M.A.E., Bakr, M.H., Bandler, J.W.: 'Adjoint higher order sensitivities for fast full-wave optimization of microwave filters', *IEEE Trans. Microw. Theory Tech.*, 2006, **54**, (8), pp. 3339–3351
14 Bandler, J.W., Cheng, Q.S., Dakroury, S.A., *et al.*: 'Space mapping: the state of the art', *IEEE Trans. Microw. Theory Tech.*, 2004, **52**, (1), pp. 337–361
15 Koziel, S., Bekasiewicz, A., Kurgan, P.: 'Rapid EM-driven design of compact RF circuits by means of nested space mapping', *IEEE Microw. Wirel. Compon. Lett.*, 2014, **24**, (6), pp. 364–366
16 Queipo, N.V., Haftka, R.T., Shyy, W., *et al.*: 'Surrogate based analysis and optimization', *Prog. Aerosp. Sci.*, 2005, **41**, (1), pp. 1–28
17 Mack, Y., Goel, T., Shyy, W., *et al.*: 'Surrogate model-based optimization framework: a case study in aerospace design', in Yang, S., Ong, Y.S., Jin, Y. (Eds.), 'Evolutionary computation in dynamic and uncertain environments' (Springer Kluwer Academic Press, 2007), vol. 51, pp. 323–342
18 Forrester, A.I., Sobester, A., Keane, A.J.: 'Multi-fidelity optimization via surrogate modelling', *Proc. R. Soc. A*, 2007, **463**, pp. 3251–3269
19 Bandler, J.W., Biernacki, R.M., Chen, S.H., *et al.*: 'Space mapping technique for electromagnetic optimization', *IEEE Trans. Microw. Theory Tech.*, 1994, **42**, (12), pp. 2536–2544
20 Koziel, S., Leifsson, L.: 'Surrogate-based modeling and optimization: applications in engineering' (Springer, 2013)
21 Koziel, S., Bandler, J.W.: 'Space mapping with multiple coarse models for optimization of microwave components', *IEEE Microw. Wirel. Compon. Lett.*, 2008, **18**, (1), pp. 1–3
22 Ismail, M.A., Smith, D., Panariello, A., *et al.*: 'EM-based design of large-scale dielectric-resonator filters and multiplexers by space mapping', *IEEE Trans. Microw. Theory Tech.*, 2004, **52**, (1), pp. 386–392

23 Koziel, S., Ogurtsov, S.: 'Design optimization of antennas using electromagnetic simulations and adaptive response correction technique', *IET Microw. Antennas Propag.*, 2014, **8**, (3), pp. 180–185
24 Robinson, T.D., Eldred, M.S., Willcox, K.E., *et al.*: 'Surrogate-based optimization using multifidelity models with variable parameterization and corrected space mapping', *AIAA J.*, 2008, **46**, (11), pp. 2814–2822
25 Koziel, S., Ogurtsov, S., Szczepanski, S.: 'Rapid antenna design optimization using shape-preserving response prediction', *Bull. Pol. Acad. Sci. Tech. Sci.*, 2012, **60**, (1), pp. 143–149
26 Koziel, S., Ogurtsov, S.: 'Rapid optimization of omnidirectional antennas using adaptively adjusted design specifications and kriging surrogates', *IET Microw. Antennas Propag.*, 2013, **7**, (15), pp. 1194–1200
27 Koziel, S., Ogurtsov, S.: 'Model management for cost-efficient surrogate-based optimization of antennas using variable-fidelity electromagnetic simulations', *IET Microw. Antennas Propag.*, 2012, **6**, (15), pp. 1643–1650
28 Koziel, S., Ogurtsov, S.: 'Multi-objective design of antennas using variable-fidelity simulations and surrogate models', *IEEE Trans. Antennas Propag.*, 2013, **61**, (12), pp. 5931–5939
29 Koziel, S., Bekasiewicz, A., Couckuyt, I., *et al.*: 'Efficient multi-objective simulation-driven antenna design using co-kriging', *IEEE Trans. Antennas Propag.*, 2014, **62**, (11), pp. 5900–5905
30 Yeung, S.H., Man, K.F.: 'Multiobjective optimization', *IEEE Microw. Mag.*, 2011, **12**, (6), pp. 120–133
31 Aljibouri, B., Lim, E.G., Evans, H., *et al.*: 'Multiobjective genetic algorithm approach for a dual-feed circular polarised patch antenna design', *Electron. Lett.*, 2000, **36**, (12), pp. 1005–1006
32 Jin, N., Rahmat-Samii, Y.: 'Advances in particle swarm optimization for antenna designs: real-number, binary, single-objective and multiobjective implementations', *IEEE Trans. Antennas Propag.*, 2007, **55**, (3), pp. 556–567
33 Bandler, J.W., Ismail, M.A., Rayas-Sánchez, J.E.: 'Broadband physics-based modeling of microwave passive devices through frequency mapping'. IEEE MTT-S Int. Microwave Symp. Digest, Boston, MA, 2000, pp. 969–972
34 Bandler, J.W., Cheng, Q.S., Nikolova, N.K., *et al.*: 'Implicit space mapping optimization exploiting preassigned parameters', *IEEE Trans. Microw. Theory Tech.*, 2004, **52**, (1), pp. 378–385
35 Coello Coello, C.A., Lamont, G.B., Van Veldhuizen, D.A.: 'Evolutionary algorithms for solving multi-objective problems' (Springer, 2007, 2nd edn.)
36 Bandler, J.W., Ismail, M.A., Rayas-Sánchez, J.E., *et al.*: 'Neuromodeling of microwave circuits exploiting space mapping technology', *IEEE Trans. Microw. Theory Tech.*, 1999, **47**, (12), pp. 2417–2427
37 Koziel, S., Echeverría-Ciaurri, D., Leifsson, L.: 'Surrogate-based methods', in Koziel, S., Yang, X.S. (Eds.) 'Computational Optimization, Methods and Algorithms' (Springer, 2011), pp. 33–60
38 CST Microwave Studio, ver. 2012, CST AG, Bad Nauheimer Str. 19, D-64289 Darmstadt, Germany, 2012
39 Agilent ADS, ver. 2011.10, Agilent Technologies, 1400 Fountaingrove Parkway, Santa Rosa, CA 95403–1799, 2011
40 Tseng, C.-H., Wu, C.-H.: 'Design of compact branch-line couplers using π-equivalent artificial transmission lines', *IET Microw. Antennas Propag.*, 2012, **6**, (9), pp. 969–974